0026-895X/09/7606-1196–1210$20.00
MOLECULAR PHARMACOLOGY
Copyright © 2009 The American Society for Pharmacology and Experimental Therapeutics
Mol Pharmacol 76:1196–1210, 2009

Vol. 76, No. 6
59139/3535523
Printed in U.S.A.

Subtype-Specific Differences in Corticotropin-Releasing Factor Receptor Complexes Detected by Fluorescence Spectroscopy

Laura Milan-Lobo,[1] Ingrid Gsandtner, Erwin Gaubitzer, Dominik Rünzler, Florian Buchmayer, Gottfried Köhler, Antonello Bonci, Michael Freissmuth, and Harald H. Sitte

Institute of Pharmacology, Center for Biomolecular Medicine and Pharmacology, Medical University Vienna, Vienna, Austria (L.M.L., I.G., F.B., M.F., H.H.S.); Max F. Perutz Laboratories, University of Vienna, Vienna, Austria (E.G., D.R., G.K.); and the Ernest Gallo Clinic and Research Center, Emeryville, and Department of Neurology, University of California, San Francisco, California (A.B.)

Received July 3, 2009; accepted September 11, 2009

ABSTRACT

G protein-coupled receptors have been proposed to exist in signalosomes subject to agonist-driven shifts in the assembly disassembly equilibrium, affected by stabilizing membrane lipids and/or cortical actin restricting mobility. We investigated the highly homologous corticotropin-releasing factor receptors (CRFRs), CRFR1 and -2, which are different within their hydrophobic core. Agonist stimulation of CRFR1 and CRFR2 gave rise to similar concentration-response curves for cAMP accumulation, but CRFR2 underwent restricted collision coupling. Both CRFR1 and CRFR2 formed constitutive oligomers at the cell surface and recruited β-arrestin upon agonist activation (as assessed by fluorescence resonance energy transfer microscopy in living cells). However, CRFR2, but not CRFR1, failed to undergo agonist-induced internalization. Likewise, agonist binding accelerated the diffusion rate of CRFR2 only (detected by fluorescence recovery after photobleaching and fluorescence correlation spectroscopy) but reduced the mobile fraction, which is indicative of local confinement. Fluorescence intensity distribution analysis demonstrated that the size of CRFR complexes was not changed. Disruption of the actin cytoskeleton abolished the agonist-dependent increase in CRFR2 mobility, shifted the agonist concentration curve for CRFR2 to the left, and promoted agonist-induced internalization of CRFR2. Our observations are incompatible with an agonist-induced change in monomer-oligomer equilibrium, but they suggest an agonist-induced redistribution of CRFR2 into a membrane microdomain that affords rapid diffusion but restricted mobility and that is stabilized by the actin cytoskeleton. Our data show that membrane anisotropy can determine the shape and duration of receptor-generated signals in a subtype-specific manner.

Signal transduction via heterotrimeric G proteins is accomplished by a cycle of activation and deactivation of the Gα-subunit, which is achieved by receptor-catalyzed exchange of prebound GDP for GTP and GTP hydrolysis by the intrinsic GTPase of Gα, respectively. Superimposed on this GTPase cycle, there is a cycle of subunit dissociation and reassociation, in which the inactive heterotrimer Gα.GDP.$\beta\gamma$ affords receptor docking, GTP binding drives subunit dissociation into Gα.GTP.Mg^{2+} and G$\beta\gamma$, and the GTPase-mediated hydrolysis promotes mutual inactivation of two Gα.GDP and G$\beta\gamma$ by reassociation of the inactive heterotrimer Gα.GDP.$\beta\gamma$. This model was established some 20 years ago, mainly by the study of reconstituted purified components (Freissmuth et al., 1989). However, since then, methods have become available that allow the tracking of the activity of individual components at the single-cell level. In several instances, these have led to observations that are incompat-

This work was supported by the Austrian Science Fund/FWF [Grants P17076, P18706, N209]; the Wiener-, Wissenschafts-, Forschungs- und Technologiefonds (MA 05); and the Gallo Research Institute and Clinics.

[1] Current affiliation: The Ernest Gallo Clinic and Research Center, Emeryville, California.

Article, publication date, and citation information can be found at http://molpharm.aspetjournals.org.
doi:10.1124/mol.109.059139.

ABBREVIATIONS: GPCR, G protein-coupled receptor; CFP, cyan fluorescent protein; YFP, yellow fluorescent protein; CRF, corticotropin-releasing factor; GFP, green fluorescent protein; CRFR, corticotropin-releasing factor receptor; C-SERT-Y, cyan fluorescent protein-serotonin transporter-yellow fluorescent protein; ECFP, enhanced cyan fluorescent protein; EYFP, enhanced yellow fluorescent protein; Y-DAT, yellow fluorescent protein-dopamine transporter; FCS, fluorescence correlation spectroscopy; FIDA, fluorescence intensity distribution analysis; FRAP, fluorescence recovery after photobleaching; TM, transmembrane; HEK, human embryonic kidney; GTPγS, guanosine 5′-*O*-(3-thio)triphosphate; MβCD, methyl-β-cyclodextrin.

ible with some of the central tenets of the model or that require the model to be adapted. For some receptors, it has been questioned, whether subunit dissociation occurs to any appreciable extent in intact cells (Hein et al., 2005). In addition, several G protein-coupled receptors have been found to form homo- and hetero-oligomers (Pin et al., 2007). In some studies, the equilibrium between monomers and dimers has been shown to be regulated by receptor activation (Cvejic and Devi, 1997; Cheng and Miller, 2001; Briddon et al., 2004). Agonist-induced changes in diffusion have been viewed as evidence for an agonist-induced disassembly of large receptor aggregates. Finally, receptors and G proteins have been found to be inhomogeneously distributed over the cell surface (Perez et al., 2006), because they may be clustered by association with anchoring molecules or trapped in specific membrane microdomains arising from the different miscibility of lipids (Chini and Parenti, 2004). It has not been clear, however, why some receptors should depend on cholesterol or on cholesterol-containing domains, whereas others do not.

We observed recently that the restricted mobility of the A_{2A}-receptor was a property specified by its hydrophobic core and contingent on the presence of cholesterol (Charalambous et al., 2008). This observation predicts that closely related receptors may be different with respect to their mobility provided that their hydrophobic cores are different in their ability to accommodate cholesterol (or other lipids). Here, we have tested this hypothesis by examining the receptors for corticotropin-releasing factor (CRF), which belong to the secretin-receptor-like family or B-family of GPCRs (Fredriksson et al., 2003). Upon binding of their endogenous ligand CRF, they preferentially engage $G\alpha_s$ and thus activate adenylyl cyclase isoforms. At high occupancy, CRFRs can also activate additional G proteins (Wietfeld et al., 2004). CRFRs are highly related, with 74% identity and 88% homology; dissimilarities are not evenly distributed; and surprisingly large degrees of divergence are observed within the transmembrane (TM) segments 1 to 4. Based on these differences, we surmised that these two receptor isoforms differed in the extent to which they formed complexes and diffused through the membrane. This conjecture was examined by recording the mobility of receptors at the ensemble level using fluorescence recovery after photobleaching (FRAP) and at the level of the individual molecule using fluorescence correlation spectroscopy (FCS) and fluorescence intensity distribution analysis (FIDA). Agonist occupancy enhanced the mobility of CRFR2 in the presence of an intact cytoskeleton. By contrast with CRFR1, CRFR2 underwent restricted collision coupling and greatly delayed internalization; disruption of the cytoskeleton by latrunculin A enhanced cAMP formation and promoted rapid internalization. Taken together, these results support a model in which the mobility of the agonist-liganded CRFR2 is restricted by actin-dependent membrane anisotropy.

Materials and Methods

Reagents. Vectors pECFP-N1 and pEYFP-N1 were from Clontech (Mountain View, CA). Human/rat CRF and α-helix CRF[9–41] were from Polypeptide (Wolfenbüttel, Germany). ^{125}I-Sauvagine was from PerkinElmer Life and Analytical Sciences (Waltham, MA). Rabbit polyclonal GFP antibody was from Clontech, anti-rabbit IgG1 horseradish was from GE Healthcare (Chalfont St. Giles, Buckinghamshire, UK). The sources of all other reagents and chemicals can be found in Charalambous et al. (2008).

cDNA Constructs and Cell Culture. The plasmids coding for mouse CRFR2β and CRFR1α were kindly provided by W. Vale (La Jolla, CA) and P. Ferrara (Basel, Switzerland), respectively. cDNAs were subcloned into pECFP-N1 and pEYFP-N1 to attach the fluorescent protein at the C terminus; the integrity of all constructs was verified by sequencing. Rab5-CFP was kindly provided by Alexander Sorkin (University of Colorado, Boulder, CO). β-Arrestin1-YFP was kindly provided by Martin Lohse (Institute of Pharmacology and Toxicology and Bio-Imaging Center, University of Würzburg, Würzburg, Germany).

HEK 293 cells were transiently or stably transfected by the Ca_2PO_4 precipitation method. For experiments using Rab5, cells stably expressing CRFR2-YFP or CRFR1-YFP were transiently transfected with Rab5-CFP. In the case of FRET experiments, all cDNAs were transiently transfected into parental HEK 293 cells. Neuronal cultures were generated from hippocampi of neonatal Sprague-Dawley rats and transfected with Lipofectamine 2000 (Invitrogen, Carlsbad, CA) after 7 days in culture.

Determination of cAMP Formation and ^{125}I-Sauvagine Binding. The formation of [^{3}H]cAMP was quantified as described previously (Kudlacek et al., 2001). The production of cAMP was stimulated by the addition of different CRF concentrations for 30 min at 37°C. Membranes were prepared from HEK 293 cells stably expressing CRFR1 and CRFR2 as in Kudlacek et al. (2001). Nuclei were removed by centrifugation (10 min at 1000*g*). Membranes were harvested at 40,000*g* for 30 min. Binding was done in a final volume of 0.1 ml containing 50 mM Tris-HCl, pH 7.5, 1 mM EDTA, 5 mM $MgCl_2$, 0.2 nM ^{125}I-sauvagine, and membrane protein (2–4 μg) for 2 to 90 min at temperatures ranging from 20 to 37°C. The reaction was terminated by filtration over GFA filters that had been presoaked in 1% polyethylenimine to reduce filter binding. Nonspecific binding was defined in the presence of the antagonist α-helix CRF[9–41]. Total binding was 4000 to 6000 cpm, and nonspecific binding amounted to ~1000 cpm and was mainly due to filter binding. Some incubations were also done in the presence of 0.1 mM GTPγS.

Fluorescence Spectroscopy. FRET microscopy was performed applying the "three-filter method" essentially as described recently (Bartholomäus et al., 2008). FRAP was recorded on a Zeiss LSM510 confocal laser scanning microscope (Carl Zeiss, Thornwood, NJ) as described previously (Charalambous et al., 2008). To allow for a better comparison, we determined the diffusion coefficient (D) using the equation $t_{1/2} = \beta\omega^2/4D$, where $t_{1/2}$ is the half-life of fluorescence recovery, ω is the radius of influence, and β is a parameter that depends on the percentage bleached (Yguerabide et al., 1982). In all measurements, β was set to 1.6, its maximum value (Yguerabide et al., 1982). All measurements were done at 22°C. The setup and cell handling for FCS has been described in detail elsewhere (Maier et al., 2005). In brief, we seeded stably transfected HEK 293 cells expressing YFP-tagged CRFRs onto poly(D-lysine)-coated Lab-Tek chamber slides (Nalge Nunc International, Rochester, NY). YFP was excited at 488 nm (argon laser line attenuated by optical density filters to avoid photobleaching and a dichroic mirror with bandpass filters). The pinhole diameter was set to 45 μm (confocal volume element, horizontal radius $\omega_1 = 0.185$ μm), as calibrated with rhodamine 6G ($D = 2.8 \times 10^{-10}$ cm^2/s). Cells were first scanned in z-direction to identify two fluorescence peaks corresponding to the upper and the lower cell surface. All measurements were subsequently recorded at the upper membrane during 10 s and at 22°C. The autocorrelation function was obtained and fitted to the equation describing a two-component model with two diffusion times, τ1 and τ2 (Maier et al., 2005). The diffusion coefficient (D) was calculated from the relation: $\tau_D = \omega_1^2/4D$. FIDA was measured using the same FCS set up; to obtain photon arrival times, the detector signal was split and guided into the correlator card and into a time measurement histogram accumulating real-time processor (Timeharp 200; PicoQuant, Berlin, Germany) triggered with 7.4 MHz. The recorded

photons were binned into 40-μs time windows. Photon-counting histograms were generated based on the probability for the occurrence of photon counts. The probability distributions were analyzed using the FIDA model according to Kask et al. (1999). The resulting brightness values relate to the tailing of the distribution on the side of higher photon counts. Details on the analysis and the calculation of the brightness can be found in a previously published equation (eq. 3 in Edetsberger et al., 2005).

Statistical Analysis. All data samples were first tested for normal distribution using the Kolmogorow-Smirnow test. Subsequently, we applied analysis of variance followed by post hoc Bonferroni's test for multiple comparisons (Fig. 2). Alternatively, if the criteria of the Kolmogorow-Smirnow test were not met, we used the nonparametric Kruskal-Wallis test with a post hoc comparison of all column pairs (Figs. 4, 5, and 7). Where appropriate, we used unpaired (Fig. 8) and paired t tests (Fig. 11).

Results

CRF Receptors Engage G_s and G_i, Form Oligomers, and Recruit β-Arrestin, but Their Ability to Undergo Internalization Is Different. We generated stably transfected HEK 293 cell lines that expressed fluorescently tagged CRFRs at comparable levels. These receptors were functionally indistinguishable from untagged receptors (data not shown); the concentration-response curves for the physiological agonist were comparable; most notably, we observed that in both CRFR1 (Fig. 1A) and CRFR2 (Fig. 1B), the concentration-response curve for agonist-induced cAMP accumulation was bell-shaped. The decrease observed at high concentrations of CRF was blunted in cells that had been pretreated with pertussis toxin. This indicates that the receptor preferentially engages G_s but that G_i isoforms (and possibly other G proteins) are also recruited at high agonist occupancy. Oligomer formation of CRFR1 and CRFR2 was investigated in living cells by FRET microscopy. CFP- and YFP-tagged receptors were transiently coexpressed in appropriate combinations; only cells displaying a CFP/YFP ratio of ~1 (mean value = 1.0 ± 0.2) were included in the analysis of N_{FRET}. We controlled our FRET measurements by the coexpression of (soluble) CFP and YFP as negative control and a dually tagged serotonin transporter, C-SERT-Y (Just et al., 2004), as a positive control. CFP and YFP displayed low background FRET (N_{FRET} = 0.08 ± 0.08; mean ± S.D.), whereas C-SERT-Y, as expected, gave a strong FRET (N_{FRET} = 0.60 ± 0.15). Energy transfer was observed between CRFR1-C and CRFR1-Y (N_{FRET} = 0.23 ± 0.10) as well as CRFR2-C and CRFR2-Y (0.35 ± 0.14; Fig. 2B). As a negative control for membrane crowding, we coexpressed CFP-tagged CRFRs and the structurally unrelated YFP-tagged dopamine transporter (DAT). These gave low N_{FRET} (CRFR1-C/YFP-DAT: 0.06 ± 0.09 and CRFR2-C/YFP-DAT: 0.13 ± 0.04; Fig. 2B) comparable with the background FRET of CFP/YFP (Fig. 2B).

Although it is clear that monomeric receptors are in principle capable of activating a G protein (Ernst et al., 2007; Whorton et al., 2007), there are several examples in which G protein activation is contingent on the dimeric form of the receptor (Hlavackova et al., 2005; Brock et al., 2007). It was therefore conceivable that receptor occupancy promoted receptor dimerization. Accordingly, we treated HEK 293 cells coexpressing CRFR1-C/CRFR1-Y and CRFR2-C/CRFR2-Y with CRF: agonist challenge did not change FRET within the CRFR1 oligomer (Fig. 2C). In contrast, FRET significantly increased in CRFR2 ($p < 0.001$) upon agonist stimulation (Fig. 2C). This was specific: incubation with the antagonist α-helical CRF[9–41] (αhCRF) did not alter N_{FRET} (data not shown). We stress, however, that the change in the FRET signal of CRFR2 oligomers may either be due to a change in the distance and/or relative orientation of the fluorophores resulting from the agonist-induced conformation or from an agonist-induced increase receptor oligomers (see FIDA below).

We used FRET microscopy to verify that agonist stimulation of both CRFR1 and CRFR2 resulted in the recruitment of β-arrestin1; it is evident from Fig. 3A that there was no appreciable difference between these two receptors (Fig. 3A). However, although agonist challenge promoted internalization of CRFR1 into Rab5-positive endosomes (Fig. 3B, top row), CRFR2 was remarkably resistant to internalization. Up to 45 min, after agonist challenge, there were only occasional internalization events (Fig. 3B, bottom row). We stress that the observation period covered very early time points and that there was no evidence for early internalization

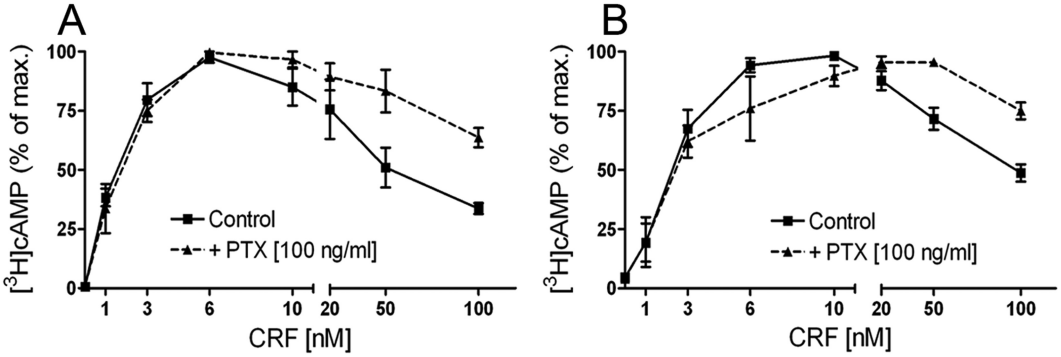

Fig. 1. Accumulation of cAMP in HEK 293 cells expressing CRF receptors. Bell-shaped concentration-response curve for CRF-induced cAMP accumulation in HEK 293 cells stably expressing the YFP-tagged versions of CRFR1 (A) or CRFR2 (B). The adenine nucleotide pool of stably transfected HEK 293 cells (2×10^5/well) was metabolically prelabeled with [^{3}H]adenine for 16 h; where indicated (triangles), cells were also maintained in the presence of pertussis toxin (100 ng/ml). Thereafter, the cells were preincubated in the presence of rolipram (100 μM) for 1 h and subsequently stimulated with the indicated concentrations of CRF for 30 min. The accumulation of [^{3}H]cAMP was quantified as outlined under *Materials and Methods*. To normalize for interassay variations, the maximum cAMP accumulation (observed with 6 and 10 nM in cells expressing CRFR1-Y and CRFR2-Y, respectively) was set to 100%. This value corresponded to 6295 ± 688 cpm and 2389 ± 176 cpm for CRFR1-Y and CRFR2-Y, respectively. Basal [^{3}H]cAMP levels were 71 ± 15 and 108 ± 7 cpm for CRFR1-Y and CRFR2-Y, respectively. Data represent means± S.E.M.; n = 3 to 8 experimental days, each concentration point measured in triplicate.

followed by rapid recycling; more pronounced internalization of CRFR2 was only seen after incubations exceeding 60 min (data not shown). Thus, CRFR1 and CRFR2, seemed to activate similar G proteins and to both recruit β-arrestin; nevertheless, they differed with respect to internalization and to the nature of the oligomeric complex.

Mobility of the CRFR Complexes at the Plasma Membrane Monitored by FRAP. The agonist-induced increase in FRET of CRFR2 may have resulted from increased accumulation of CRFR2 in oligomeric complexes or a decline in fluorophore distance and/or rotational mobility in existing oligomers. An increase in the size of the oligomeric complex should result in a change in mobility. We tested this possibility by comparing the mobility of YFP-tagged CRFR1 and CRFR2 stably expressed in HEK 293 cells by FRAP. The fluorescence was uniformly distributed over the cell surface. A membrane strip of ~5 μm was photobleached, and recovery of fluorescence was monitored to estimate the lateral mobility of the receptors (Fig. 4B). In the absence of agonist, CRFR1 and CRFR2 were not different in their mobility: maximal recovery was approximately 60% of prebleach values (empty symbols at the bottom of Fig. 4B), and half-maximal recovery was achieved after ~15 s resulting in a diffusion coefficient of $2.3 \pm 0.9 \times 10^{-9}$ and $2.3 \pm 0.8 \times 10^{-9}$ cm^2/s for CRFR1 and CRFR2, respectively (mean ± S.D.; Fig. 3B). Then cells were incubated with different concentrations of the agonist CRF for 15 min. During this time and with the highest concentration used (100 nM), some internalization was seen for CRFR1, but the bulk of the receptors was still present at the plasma membrane to allow for fluorescence recovery (Fig. 4B). In contrast, CRFR2 did not internalize during the first 40 min of agonist challenge (Fig. 3B). Accordingly, all recordings were done within 15 min of agonist challenge to minimize confounding effects arising form internalization. Agonist activation did not significantly affect the diffusion coefficient of CRFR1 (Fig. 4B, left). In contrast, agonist activation of CRFR2-Y significantly increased the diffusion coefficient (Fig. 4B, right). This effect was specific for the agonist because a saturating concentration of antagonist did not affect the mobility of CRFR2-Y (Fig. 4B, right). Cells were pretreated for 1 h with latrunculin A to disrupt cortical actin filaments: this manipulation did not affect the lateral mobility but abolished the agonist-induced increase in mobility of CRFR2 (Fig. 4B, right). Agonist activation of CRFRs also affected the extent of maximal fluorescence recovery (i.e., the mobile fraction) (Fig. 4C). This effect was most pronounced for CRFR2-Y: a statistically significant decrease in the mobile fraction was seen in the presence of both

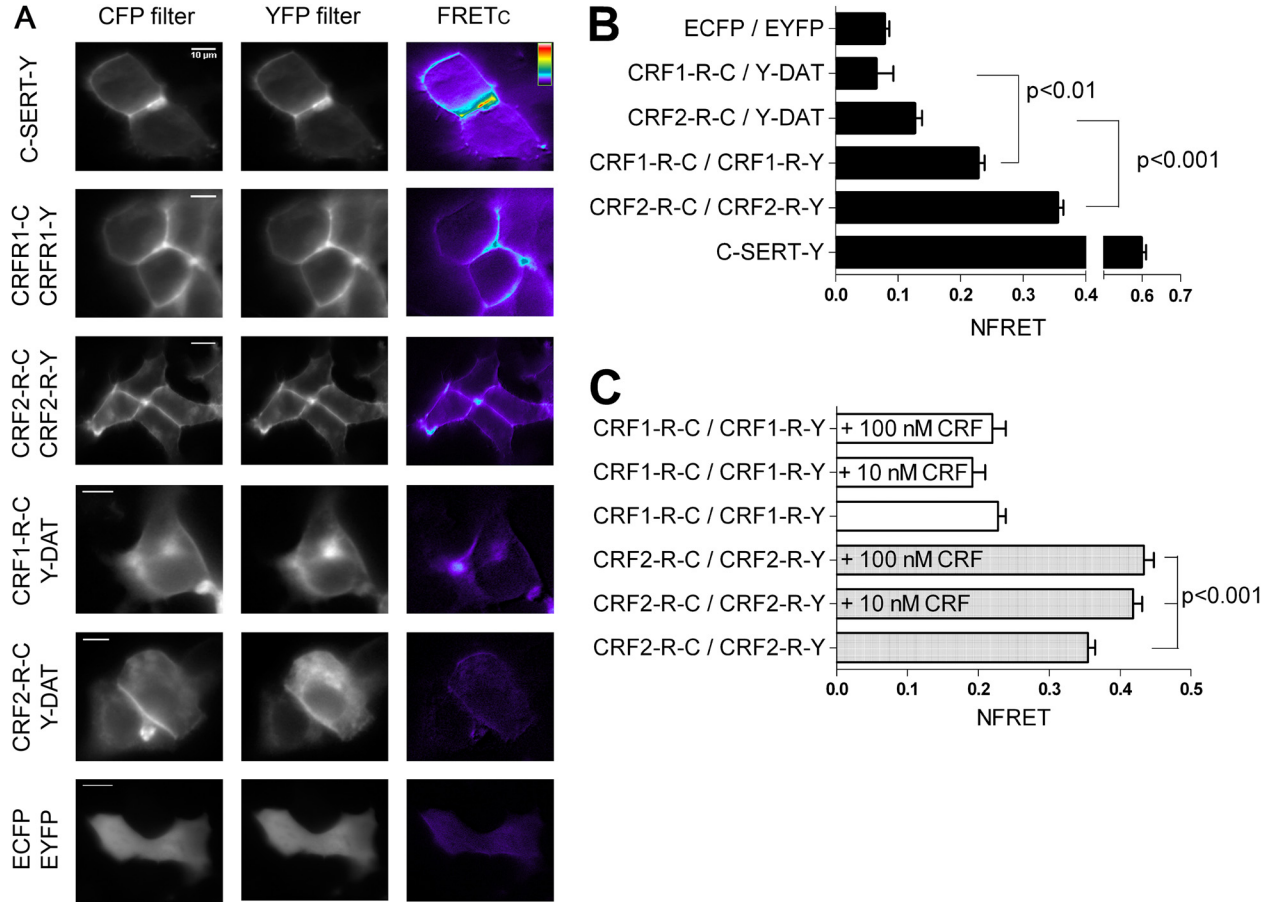

Fig. 2. FRET microscopy of CRF-receptors. A, HEK 293 cells transiently expressed plasmids encoding CFP- or YFP-tagged proteins as indicated. The columns show CFP and YFP images as indicated, the third column shows a false color rendering of the bleed-through-corrected FRETc image. All images are representative of two to seven experimental days and corrected for background. Scale bar, 10 μm. B, N_{FRET} values were calculated as described previously (Bartholomäus et al., 2008); cells expressed the indicated constructs: ECFP + EYFP (n = 106 cells), CRFR2-C + Y-DAT (n = 13), CRFR1-C + Y-DAT (n = 11), CRFR2-C + CRFR2-Y (n = 220), CRFR1-C + CRFR1-Y (n = 90), and C-SERT-Y (n = 124). C, N_{FRET} values were determined in cells expressing the indicated CRFR-isoforms: CRFR2-C and CRFR2-Y in the absence (n = 220 cells) and presence of CRF (10 nM, n = 103; 100 nM, n = 83); similarly, CRFR1-C and CRFR1-Y in the absence (n = 90) and presence of CRF (10 nM, n = 27; 100 nM, n = 26).

10 and 100 nM CRF but not in the presence of the antagonist or of latrunculin A (Fig. 4C, right). However, the mobile fraction of CRFR1 also decreased in a statistically significant manner in the presence of CRF (Fig. 4C, left). This decrease may be rationalized by taking into consideration the agonist-induced internalization of CRFR1, but it is not readily evident why the mobile fraction of CRFR2 should decrease upon agonist occupancy because this receptor did not internalize to an appreciable extent (Fig. 3B). Finally, it is also worth mentioning that fractional recovery was lower in CRFR2 than in CRFR1.

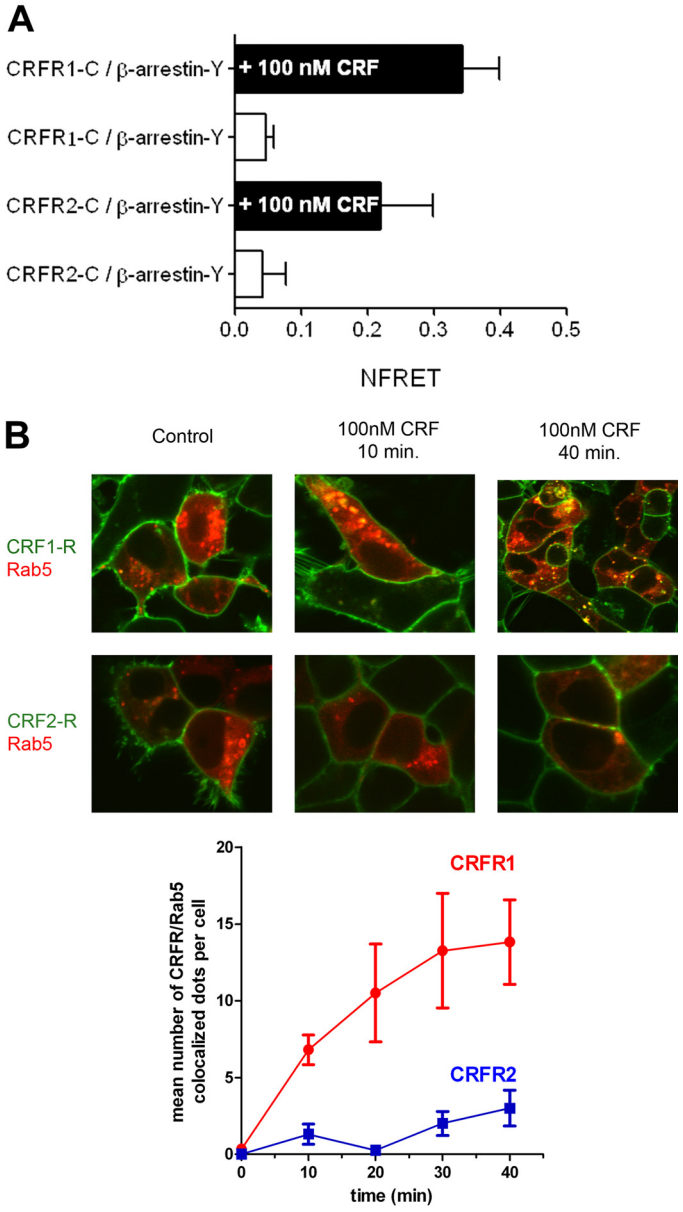

Fig. 3. CRFRs interact with β-arrestin and internalize upon agonist treatment. A, HEK 293 cells transiently expressed plasmids encoding CFP-tagged CRFRs or YFP-tagged β-arrestin1. FRET microscopy was performed in the absence (□) or presence of agonist CRF (■; [CRF] 100 nM) as described under *Materials and Methods*; NFRET values were determined as described previously (Bartholomäus et al., 2008). Data represent means ± S.E.M. (n = 7, two independent transfections). B, confocal images of HEK 293 cotransfected with either CRFR1 or CRFR2 tagged with YFP (displayed in green color) and Rab5 tagged with CFP (displayed in red color). Yellow coloring indicates colocalization of YFP- and CFP-tagged proteins (at control conditions and after incubation with 100 nM CRF at the times indicated). The images are representative of three experimental days. The colocalization of CRFRs and of Rab5 was scored by an observer blinded to the experimental condition. Cells (6–11) from different experiments were scored per time point. The resulting average density of receptor positive vesicle/optical section of a given cell was plotted as a function of time. Error bars represent S.E.M.

Diffusion Coefficient for CRFR Subtypes Determined by FCS. The FRAP experiments summarized above indicate that agonist stimulation increased the mobility of CRFR2 and caused immobility of at least some of these complexes. FRAP analysis only allows for a global estimate of protein mobility because it averages the movement of a large number of molecules (i.e., ensemble behavior). Hence, it does not allow for the understanding of the distribution of mobilities of individual fluorescent species: this was explored by using FCS (Bacia and Schwille, 2003; Chen et al., 2006). For FCS measurements, the confocal volume was positioned at the top membrane of a HEK 293 cell stably expressing CRFR1 or CRFR2; the fluctuations in fluorescence were recorded for 10 s. The analysis of the resulting autocorrelation curves for CRFR1 (Fig. 5A, left) and for CRFR2 (Fig. 5A, right) revealed that the data were best described by a model assuming the presence of two fluorescent species. The first component revealed a diffusion time (τ1) of ~0.15 ms; this is too fast for a membrane protein (Barak et al., 1997; Adkins et al., 2007). Such rapidly diffusing species are commonly observed in FCS microscopy and most likely correspond to "on/off" fluorescence flickering of free YFP molecules (Haupts et al., 1998; Pucadyil et al., 2004; Philip et al., 2007). Free YFP molecules were indeed detected in cell lysates (see below, Fig. 7B). In contrast, the second component (τ2) extracted from the generating function was consistent with the (membrane-embedded) fluorescently tagged CRFR complex. It is evident from Fig. 4B that there was a large variation in the mobility of individual fluorescent receptor species in both CRFR1- and CRFR2-expressing cells. On average, rapidly moving species of CRFR1 were slightly more abundant than those of CRFR2 under basal conditions. However, increasing concentrations of CRF augmented the proportion of rapidly moving CRFR2-Y, resulting in a significant increase in average mobility (e.g., diffusion coefficient D_2 of CRFR2 = 5.8 ± 3.4 × 10^{-9} cm^2/s in the presence of 100 nM CRF; Fig. 5B, right). This effect was contingent on the agonist activity of CRF: it was not elicited by saturating concentrations of the antagonist, which, however, blocked the CRF effect (D_2 = 5.7 ± 3.9 × 10^{-9} cm^2/s). CRF specifically affected the mobility CRFR2 because it did not alter the relative distribution of rapidly and slowly moving CRFR1 species (Fig. 5B, left). Analogous data were obtained in hippocampal neurons expressing CRFRs (Fig. 6). We noted that the diffusion rate in hippocampal neurons was consistently faster than in HEK 293 cells (compare Figs. 5 and 6). For obvious reasons, hippocampal neurons were transiently transfected to express the receptors. We therefore verified that the level of CRFR expression did not affect the lateral mobility. We compared three different cell lines stably expressing CRFR2; the expression level in these cells varied ≫20-fold, requiring different exposure times to visualize the immunoreactive bands (Fig. 7B); the range of expression of CRFR2 comprised the expression level of CRFR1 (Fig. 7B, right lane labeled 4). Despite this large variation in expression level, the FCS recordings were virtually superimposable. (Fig. 7A). It is also evident that immunoreactive degradation products were

present, most notably a band at 25 kDa corresponding to free YFP (open arrow in Fig. 7B), which, as mentioned earlier, accounted for the rapidly diffusing component resolved in the generator function.

The Agonist-Induced Shift in Mobility of CRFR2 Is Contingent on Cortical Actin Filaments and Cholesterol. CRFR1 and CRFR2 are believed to regulate identical effectors; however, it is conceivable that the mobility of a

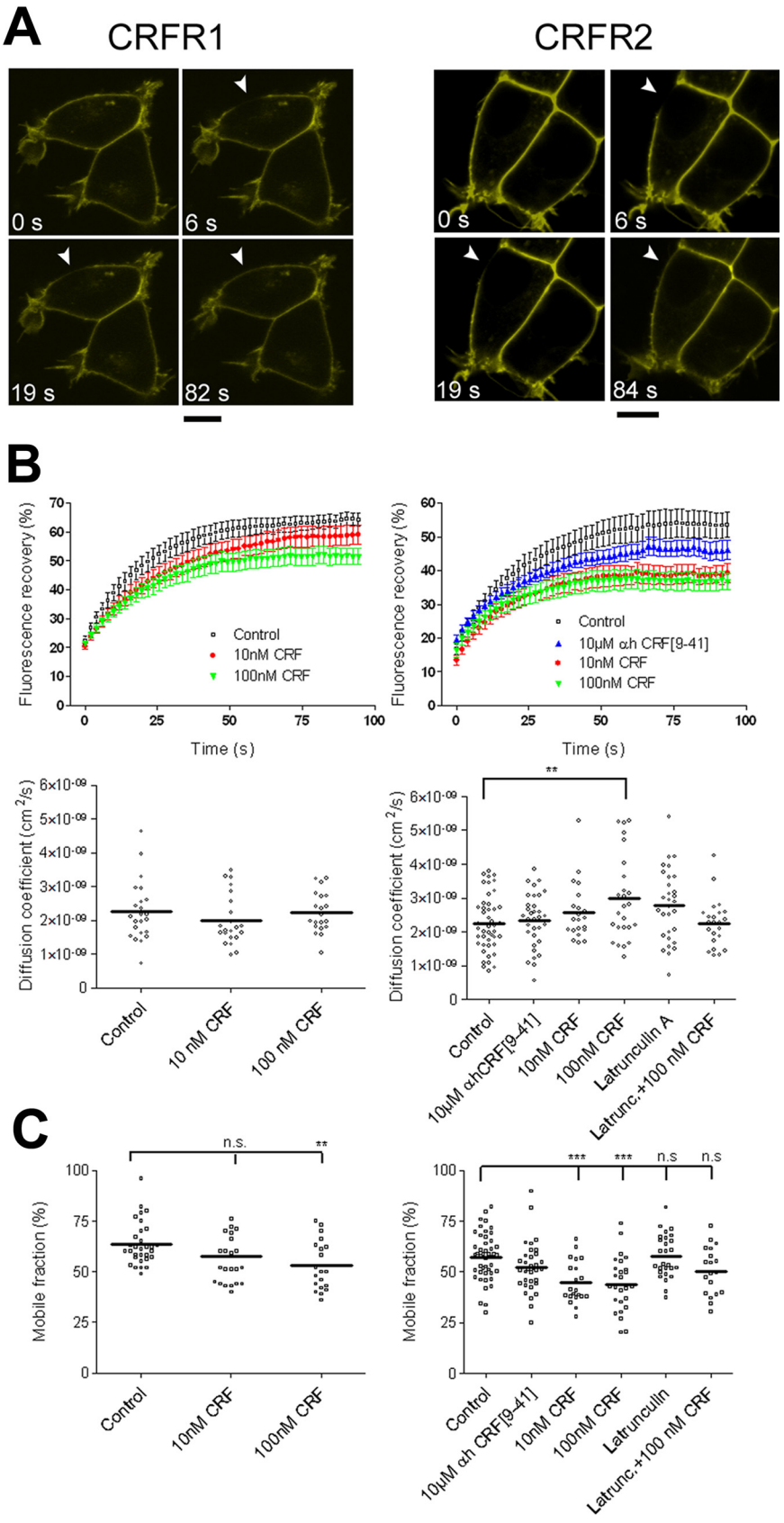

Fig. 4. FRAP microscopy of CRF-receptors. A, confocal images of stably transfected HEK 293-CRFR1-Y or HEK 293-CRFR2-Y cells, representative of three to six experimental days. After an initial cell scan (0 s), a region of interest (arrow) was photobleached, and the recovery of the fluorescence was monitored over 90 s. The normalized fluorescence recovery was plotted versus time as an example of 1 experimental day and fitted by nonlinear regression (see *Materials and Methods*; basal: $n = 9$, 10 nM CRF: $n = 7$ and 100 nM CRF: $n = 7$, 10 μM concentration of antagonist αhCRF[9–41]: $n = 11$). The length of the photobleached strip was 5.5 ± 0.4 μm. B, scatter plots of the diffusion coefficients (n = 20–30 cells for CRFR1; n = 21–88 cells for CRFR2). C, scatter plots of the mobile fractions for each receptor subtype under the same conditions described before. Horizontal lines represent the mean. **, $p <$ 0.01 and ***, $p < 0.001$; n.s., not significant. Scale bar, 10 μm.

large proportion of CRFR2 is locally confined by the cytoskeleton, i.e., cortical actin filaments. In this model, agonist stimulation of CRFR2 generates a signal that reshapes the cytoskeleton and thus allows for rapid diffusion of previously immobile receptors. In FRAP experiments, the basal mobility of CRFR2-Y was not affected by treating the cells with latrunculin A. Both the diffusion coefficient (Fig. 4B, right) and the mobile receptor fraction (Fig. 4C, right) were similar to those observed under control conditions. FRAP records ensemble changes in mobility; given the large variation in individual mobilities (Fig. 5), it is not surprising that FRAP is less sensitive than FCS. Accordingly, we also assessed the effect of latrunculin A on receptor mobility by FCS: lateral mobility of the receptors was not affected per se, but it abrogated the agonist-induced appearance of rapidly moving species. Hence, the average mobility was unchanged (Fig. 8B). These observations are inconsistent with receptor-induced remodelling of actin filaments, but they are indicative of a more fundamental source of membrane anisotropy and/or receptor heterogeneity (i.e., one that cannot be solely accounted for by microdomains created by the submembranous cytoskeleton).

Cholesterol is believed to be distributed inhomogeneously over the membrane. A possible contribution thereof was tested by depleting or clustering cholesterol with methyl-β-cyclodextrin and filipin3, respectively. Pretreatment of cells with these substances caused a significant shift in the distribution of CRFR2 mobility with a preponderance of slowly migrating species resulting in low average diffusion coefficients (Fig. 8). It is important to note that stimulation with CRF did not result in an increase in the lateral mobility of

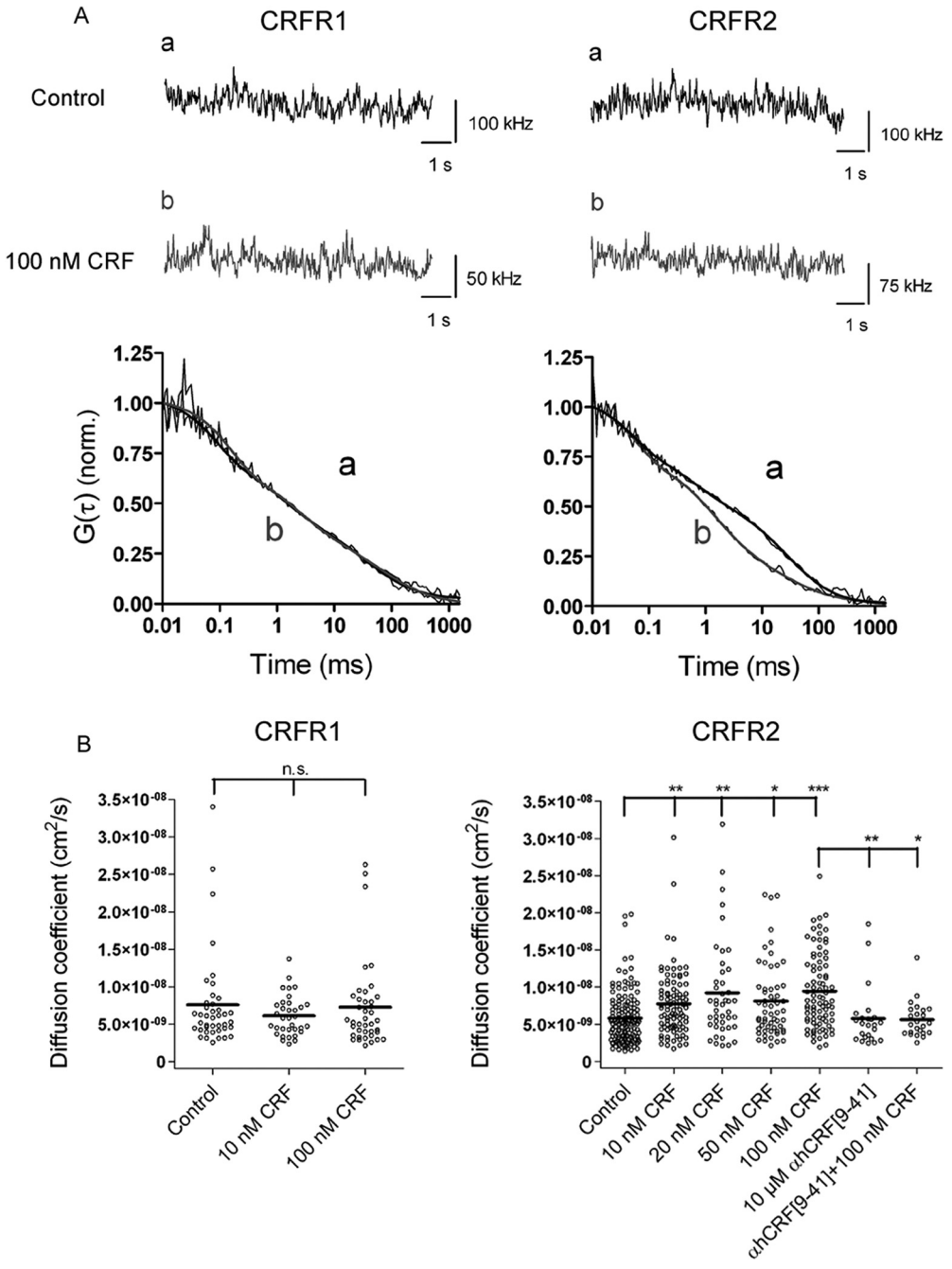

Fig. 5. FCS recordings of CRFRs stably expressed in HEK 293 cells. A, representative recordings of the intensity fluctuations (top) of CRFR1-Y and CRFR2-Y in the absence (black curve, a) and presence of 100 nM CRF (gray curve, b). Autocorrelation curves (bottom) calculated from the intensity fluctuations (in kilohertz) were fitted to a two-component model and normalized (raw count rates; control conditions: CRFR1-Y = 238 kHz, CRFR2-Y = 239 kHz; 100 nM CRF: CRFR1-Y = 131 kHz, CRFR2-Y = 170 kHz). Under control conditions, the two components have diffusion times of $\tau 1$ ~0.13 ms and $\tau 2$ ~15.6 ms for CRFR1-Y cells and $\tau 1$ ~0.15 ms and $\tau 2$ ~20.5 ms for CRFR2-Y cells. B, scatter plots represent the diffusion coefficient of both CRFRs after incubation (15 min) in the absence and presence of CRF or 10 μM antagonist (αhCRF[9–41]); 3 to 13 experimental days, n = 41 to 140 cells. Horizontal lines represent the mean; *, $p < 0.05$; **, $p < 0.01$; and ***, $p < 0.001$; n.s., not significant.

CRFR2 under these conditions (Fig. 8B). Readdition of cholesterol antagonized the actions of methyl-β-cyclodextrin (data not shown; Charalambous et al., 2008). We also attempted to resolve different populations of receptors by density gradient centrifugation. However, although it was possible to isolate detergent resistant-membranes (i.e., membrane proteins resistant to extraction by Triton X-100) on sucrose gradients, these failed to reveal a different distribution of CRFR1 and CRFR2 regardless of whether the cells were stimulated with agonist or preincubated with antagonist before cell lysis (data not shown).

Changes in Lateral Mobility Are Not Accounted for by Changes in Size of CRFR2 Receptors. The higher lateral mobility of CRFR2 receptors observed after ligand binding cannot explain the results obtained by FRET microscopy: agonist incubation augmented FRET in CRFR2 homo-oligomers. One possible explanation is to assume increased accumulation of CRFR2 in oligomeric complexes. The changes in mobility (recorded by FRAP and FCS) provided circumstantial evidence against this explanation. The alternative interpretation is to posit that the oligomeric nature of the receptor is not affected by agonist treatment, but the mobility is altered by the agonist because the receptor complexes are released (e.g., from tethering molecules or redistributed into membrane areas with increased fluidity). The two hypothetical explanations can be differentiated by using FIDA (Fig. 9) because the number of photons emitted by a diffusing entity is determined by its number of fluorophores (Kask et al., 1999). Accordingly, the presence of two species of distinct size should be reflected in the distribution of emitted

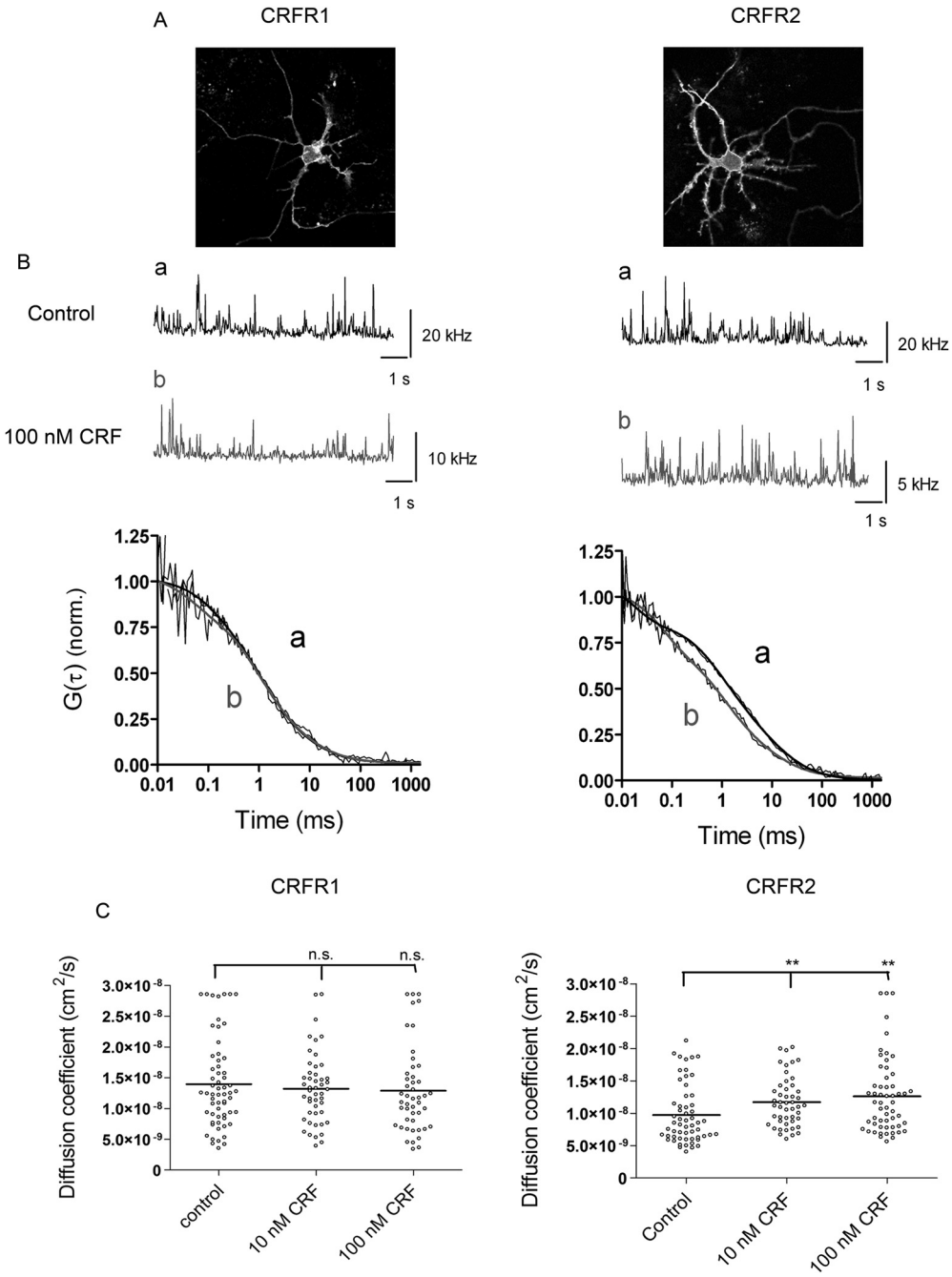

Fig. 6. FCS recordings of CRFRs expressed in hippocampal neurons. A, representative measurements of the intensity fluctuations (top two) of YFP-tagged CRFR1 and CRFR2 in transiently transfected hippocampal neurons. The measurements were done in the absence (black curve, a) and presence of 100 nM CRF (gray curve, b) and are representative of three experimental days. Autocorrelation curves (bottom) were calculated from the intensity fluctuations (in kilohertz); the curves were fitted to a two component-model and normalized (raw count rates; control conditions: CRFR1-Y = 11 kHz, CRFR2-Y = 8 kHz; 100 nM CRF: CRFR1-Y = 4 kHz, CRFR2-Y = 2.5 kHz). The two components have diffusion times of $\tau 1 \sim 0.013$ ms and $\tau 1 \sim 8.1$ ms for CRFR1 control cells and $\tau 1 \sim 0.018$ ms and $\tau 2 \sim 10.6$ ms for CRFR2 control cells. B, bar chart represents the diffusion coefficient of each receptor subtype at different concentrations of CRF; n = 30 to 62.

photons over time. However, the photon-counting histograms depicted in Fig. 9 were all adequately described by a probability distribution for a single species: regardless of whether the cells had been incubated in the absence (Fig. 9A, top) or presence of agonist (Fig. 9A, bottom), the fit was not improved by assuming the presence of a second species, and this was true for both CRFR isoforms (Fig. 9B).

CRFR1 and CRFR2: Restricted versus Unrestricted Collision Coupling. Taken together, the observations are consistent with the following hypothetical model: CRFR2 undergoes an agonist-induced redistribution into a membrane compartment that allows for fruitful coupling with its cognate G proteins(s). G_s is believed to be also subject to anisotropic distribution in the plasma membrane (Allen et al., 2007). In the agonist-liganded state, the long-range mobility of CRFR2 may be restricted by the actin cytoskeleton. In contrast, CRFR1 may sample the large areas of the membrane with unrestricted mobility. Experiments designed to test the mode of G protein-coupling are carried out under cell culture conditions (i.e., at 37°C); FCS recordings and FRAP experiments, however, were done at 22°C. Depending on the lipid composition of the membrane, it is conceivable that the fluidity of the membrane changes over this temperature range, and this may affect signal transfer from receptor via G protein to the effector (Whetton et al., 1983). With our setups, it has not been possible to record receptor mobility at 37°C: temperature gradients resulted in abrupt and unpredictable shifts in the focus plane. As an alternative, we examined receptor-G protein coupling at different temperatures by using high-affinity agonist binding (which is contingent on ternary complex formation of agonist-receptor and G protein; Freissmuth et al., 1989). CRFR1 and CRFR2 were labeled with the high-affinity agonist ^{125}I-sauvagine, and the association rate was determined at temperatures ranging from 20 to 37°C (shown for CRFR1 in Fig. 10A). Binding was greatly reduced by the addition of GTPγS (Fig. 10A, △), indicating that binding tracked ternary complex formation. It is evident from Fig. 10B that the Arrhenius plot was linear over the temperature range studied; there was no evidence for a break point that would be indicative of a phase transition. Finally, the slopes of the Arrhenius plots were in a range comparable with those determined previously (Waldhoer et al., 1999).

The model of distinct mobilities of CRFR1 and of CRFR2 posits that because of its restricted mobility, CRFR2 may only interact with G proteins in its close vicinity, resulting in restricted collision coupling. We used two approaches to this model: 1) we varied receptor expression levels; and 2) we examined the effect of disrupting the actin cytoskeleton on the agonist-induced response. The expression level of CRFR2 and CRFR1 was varied 5-fold, and the agonist-induced cAMP accumulation was measured in pertussis toxin-treated cells to obviate confounding effects arising from the recruitment of G_i at high agonist occupancy (Fig. 1). In restricted collision coupling, increased levels of receptor expression translate solely into an increased maximum effect (E_{max}). In contrast, the EC_{50} for the agonist does not change because of the

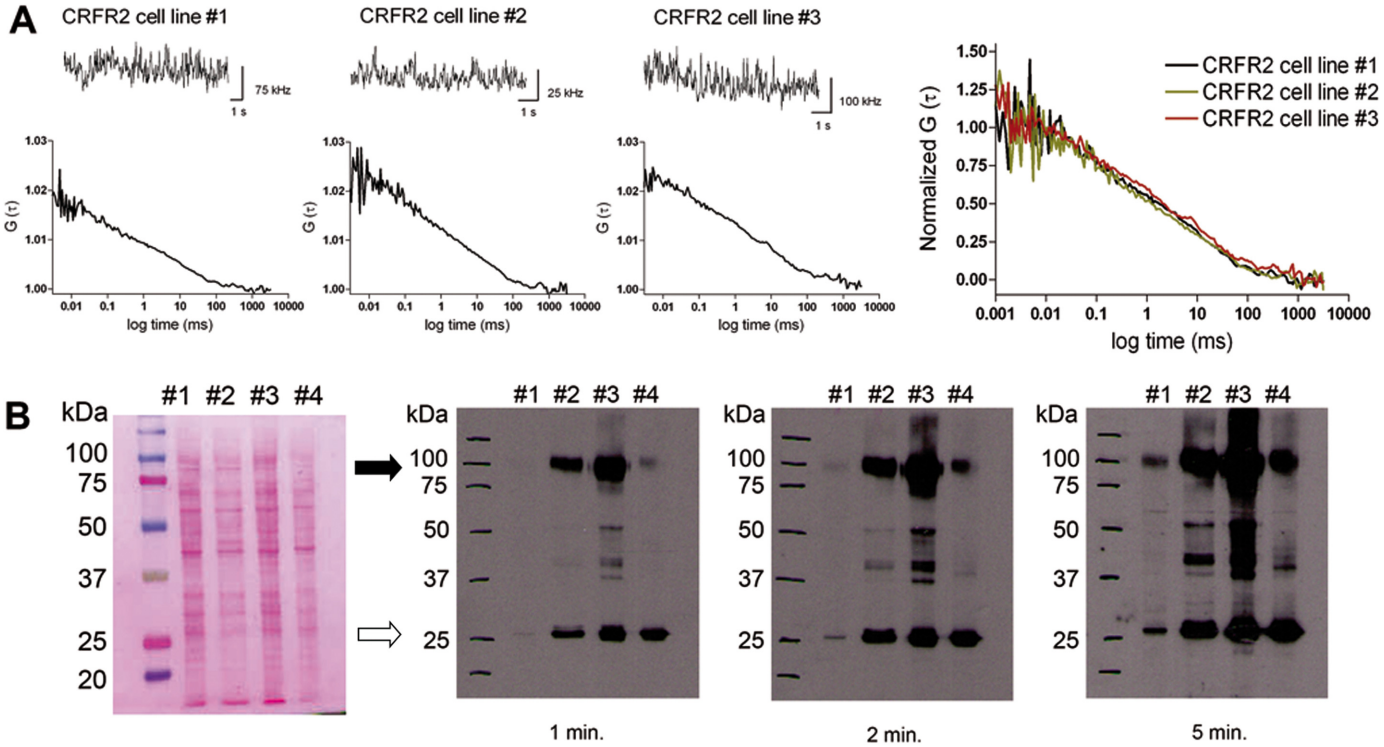

Fig. 7. FCS recordings in HEK 293 cell lines expressing different levels of CRFR2. A, representative measurements of the intensity fluctuations (top) of three cell lines stably expressing CRFR2-Y (denoted 1 to 3). Autocorrelation curves (bottom) were calculated from the intensity fluctuations (in kilohertz) and fitted to a two-component model. Right, the curves were superimposable. B, receptor levels visualized by immunoblotting; lysates (~7 μg of protein) were prepared from the three cell lines (1–3) used in A and from the CRFR1-expressing cell (4) for comparison; after separation on a denaturing SDS-polyacrylamide gels, proteins were electrophoretically transferred onto nitrocellulose membranes, stained with Ponceau-S (right), and the immunoreactivity was subsequently visualized with an anti-GFP antibody (1:5000) by enhanced chemiluminescence using three different exposure times (indicated under each blot) to account for the large difference in expression levels. Note that differences in loading do not account for the different levels of immunoreactivity. The closed and open arrows indicate immunoreactivity for CRFRs and free YFP, respectively. Data are from one representative experiment that was replicated with identical results.

limited number of G proteins engaged by a spatially restricted receptor. However, increased receptor levels translate into a leftward shift of the concentration-response curve for the agonist due to the built-in signal amplification of unrestricted collision coupling. It is evident from Fig. 11 that agonist potency (i.e., EC_{50} for CRF) varied with the expres-

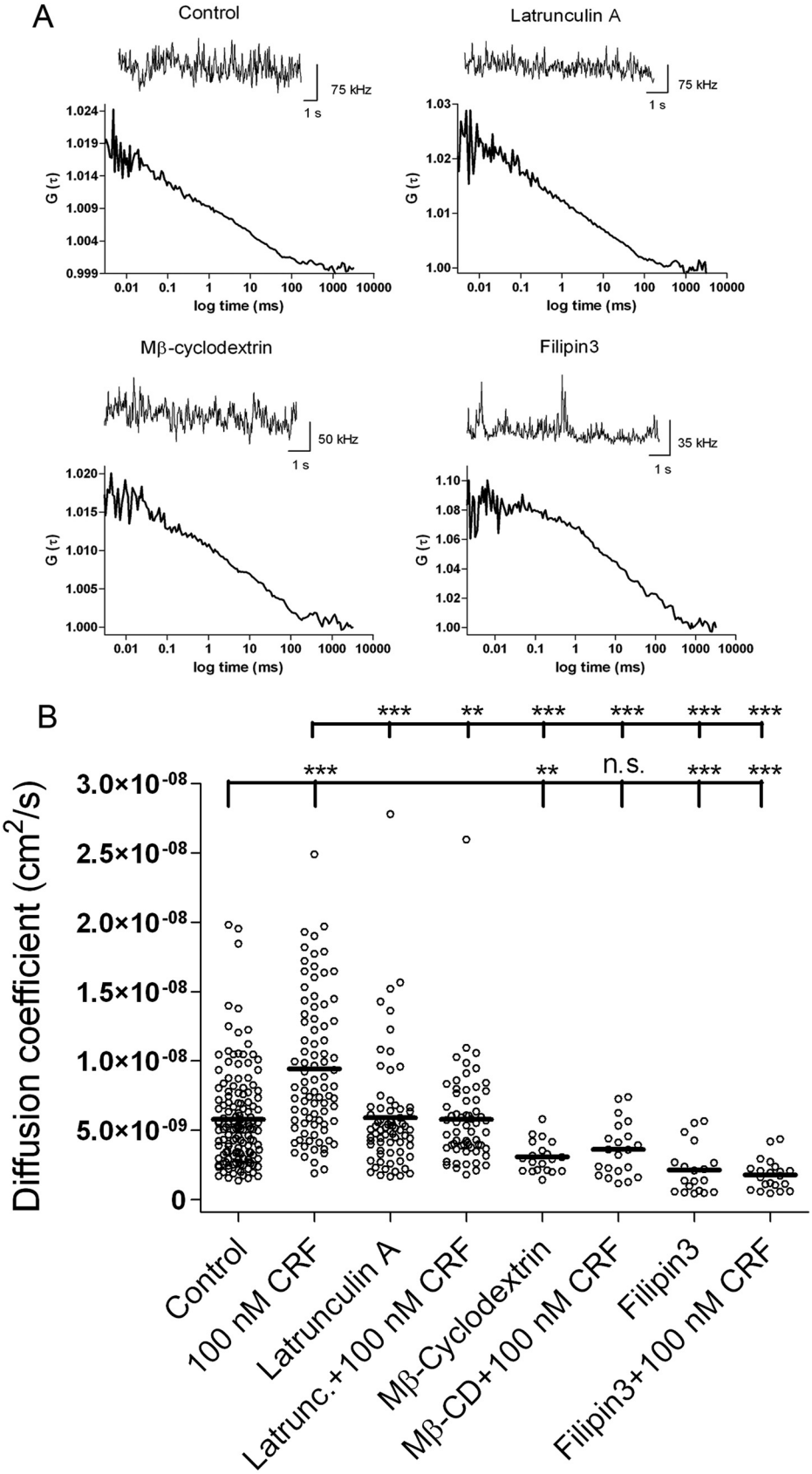

Fig. 8. Mobility of CRFR2-Y after disruption of cortical actin and cholesterol depletion/clustering assessed by FCS. A, representative measurement of the intensity fluctuations (top) of CRFR2-Y cells and after treatment with latrunculin A (1 μM), MβCD (8 mM), and filipin3 (5 μg/ml). Autocorrelation curves (bottom) calculated from the intensity fluctuations (in kilohertz) were fitted to a two-component model yielding diffusion times of CRFR2 τ2: ~20.5, ~22, ~31.6, and ~92.5 ms for control, latrunculin A-, MβCD-, and filipin3-treated cells, respectively. B, scatter plots represent the diffusion coefficient of CRFR2-Y after incubation with CRF, latrunculin A (n = 70), MβCD (n = 20), or filipin3 (n = 19). Horizontal lines represent the mean; **, $p < 0.01$; and ***, $P < 0.001$; n.s., not significant.

sion level of CRFR1 (Fig. 11A) but not with CRFR2 (Fig. 11B). Conversely, disrupting the cytoskeleton with latrunculin increased the response to CRFR2 receptor in the intermediate concentration-range (Fig. 11D) but did not affect the concentration-response curve for agonist at CRFR1 (Fig. 11C). Microtubules are also believed to participate in the organization of signaling complexes (Allen et al., 2007). Disruption of microtubules by the depolymerizing agent colchicine for instance has been shown to blunt adenylyl cyclase stimulation via G_s (Head et al., 2006). As shown in the inset to Fig. 11, C and D, this can also be recapitulated with CRF-mediated cAMP-accumulation; however, signal transfer from CRFR1 and CRFR2 is impaired to a similar extent. We stress that the experiments summarized in Fig. 11, C and D, were carried out in stably transfected cells that expressed equivalent levels of receptors.

Disrupting the Actin Cytoskeleton Promotes Internalization of CRFR2. Upon binding of agonist CRFR2 recruits β-arrestin but fails to undergo internalization; we surmised that this deficiency was linked to the altered mobility of the agonist-liganded receptor, because the receptor entered into a compartment that shielded it from the internalization machinery. Accordingly, we pretreated stably transfected cells that expressed equivalent levels of CRFR1 and CRFR2 and challenged these with agonist. As expected, internalization of CRFR1 was seen in both the absence (Fig. 12, top row) and presence (Fig. 12, second row) of latrunculin. Likewise, agonist stimulation did not trigger internalization CRFR2 under control conditions (Fig. 12, third row). In contrast, in latrunculin-treated cells (Fig. 12, bottom row), CRFR2 was as rapidly and as efficiently internalized as CRFR1. Thus, the phenotypic

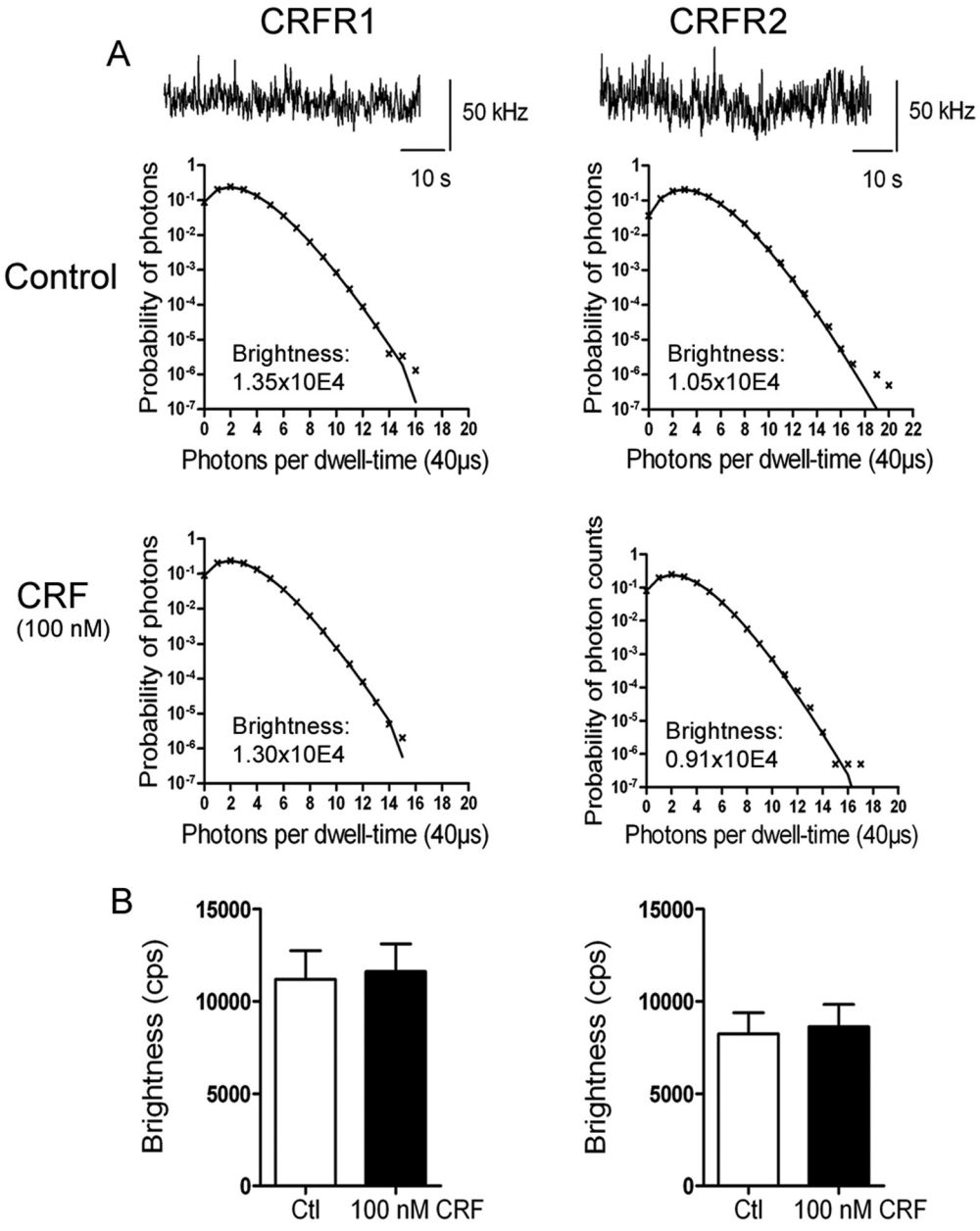

Fig. 9. CRFR complexes examined by FIDA. A, representative measurements of the intensity fluctuations (in kilohertz) detected by FCS (top) of CRFR1-Y and CRFR2-Y were used to calculate the probability of the photons detected by the microscope per 40 μs. A photon-counting histogram is shown for CRFR1-Y and CRFR2-Y in the presence or absence of 100 nM CRF. All measurements were best fitted with a single component model, and the brightness of each was determined as described under *Materials and Methods*. B, bar chart representing the brightness calculated for CRFR1-Y and CRFR2-Y at control conditions and 100 nM CRF of (two experimental days). Bars represent mean, S.E.M., n = 18 to 25 cells.

differences between CRFR2 and CRFR1 were eliminated by disrupting the cytoskeleton.

Discussion

It is generally accepted that GPCRs can exist both in monomeric and oligomeric form, but it has remained contentious whether agonists affect the monomer-oligomer equilibrium (Pfleger and Eidne, 2005). There are two approaches that have been used to address the issue. First, methods that focus on changes in resonance energy transfer between fluorescently labeled receptor moieties have been used. Increases or decreases in resonance energy transfer, however, do not provide any unequivocal evidence for a change in the oligomer/monomer equilibrium, because energy transfer does not only depend on the distance of the fluorophores but on their relative orientation and their rotational freedom. This information is accessible by measuring recording polarized light emission. A systematic survey shows that this has not been used to differentiate between agonist-induced changes in monomer/dimer equilibrium and agonist-induced conformational changes (Pfleger and Eidne, 2005). Second, the mobility of the receptor particle can be tracked. An accelerated mobility is typically viewed as evidence for a dissociation of large complexes (e.g., of the δ-opioid receptors) (Cvejic and Devi, 1997). On the other hand, the formation of higher-order oligomers has been ascribed to a slowly diffusing receptor population (Philip et al., 2007). Our observations do not support any of these interpretations for CRF receptors: analysis of brightness by FIDA unequivocally demonstrates that the size of the receptor species remains constant regardless of the presence or absence of agonist. Several arguments suggest that a change in oligomeric assembly could have been detected in our experiments, if it had occurred: 1) CRFR1 and CRFR2 were present as oligomers at the plasma membrane; 2) CRF enhanced FRET in CRFR2; 3) FCS detected a large variation in the mobility of individual fluorescent receptor molecules; and 4) agonist activation induced a clearcut shift in this distribution of CRFR2 diffusion rates. Thus, we conclude that CRFRs are constitutive oligomers of fixed stoichiometry, which is not subject to agonist regulation. This interpretation is in line with the current evidence that suggests that the oligomeric state of secretin receptor-like/class B GPCRs is not subject to regulation by agonist occupancy (Pfleger and Eidne, 2005).

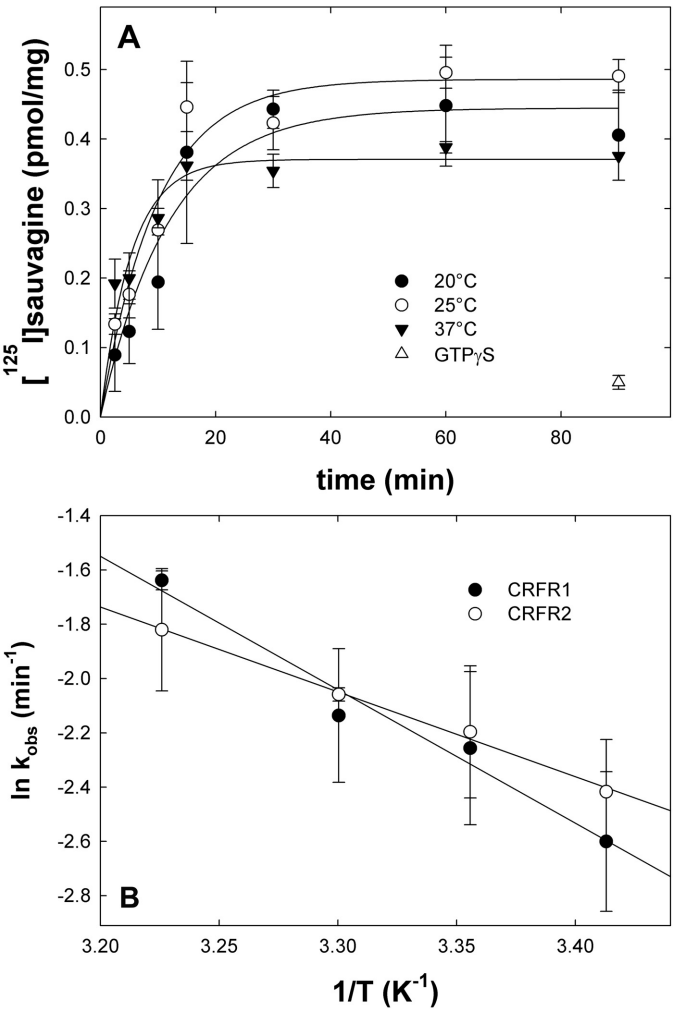

Fig. 10. Time course of ^{125}I-sauvagine binding to membranes prepared from CRFR1 and CRFR2 expressing cells at different temperatures. A, membranes from HEK 293 cells expressing CRFR1 (2–4 μg/assay) were incubated for the indicated time intervals and at the indicated temperatures in the presence of 0.2 nM ^{125}I-sauvagine. A parallel incubation contained 0.1 mM GTPγS (△), which reduced binding to a similar extent at all temperatures studied. Data are means ± S.D. from three independent experiments carried out in duplicate. A similar experiment was also done at 30°C but the points were omitted for the sake of clarity. The solid lines were drawn by fitting the data points to an equation describing a monoexponential association. B, Arrhenius plot. Apparent on rates determined were obtained as outlined in A for CRFR1.

Although CRFR1 and CRFR2 are closely related and couple to the same set of G proteins, they differed in their response to CRF in three respects: 1) agonist-induced changes in receptor mobility were seen with CRFR2 but not with CRFR1; 2) CRFR1 but not CRFR2 was internalized upon agonist binding; 3) the EC_{50} for agonist activation of CRFR2 was independent of receptor levels, a finding consistent with restricted collision coupling. We argue that all three phenomena are related and provide circumstantial evidence for the conjecture that upon agonist binding, CRFR2 enters a different membrane microdomain in which its movement is spatially restricted. These membrane domains are maintained by the actin cytoskeleton: upon entering into this microdomain, agonist-bound CRFR2 diffuses more rapidly but within a limited range. This interpretation is supported by the observation that agonist binding reduced the mobile fraction of CRFR2, which was prevented by latrunculin pretreatment. Accordingly, agonist-liganded CRFR2 has only access to a limited number of G_s molecules and is spatially segregated from the internalization machinery. Hence, it fails to undergo internalization, although β-arrestin is readily recruited to CRFR2. Alternatively, CRFR2 may fail to undergo internalization because it is tethered to the actin cytoskeleton, which can limit the propensity of receptors to undergo internalization (Puthenveedu and von Zastrow, 2006). This alternative explanation is unlikely, because it cannot account for the agonist-induced accelerated diffusion rates.

Agonist stimulation increased the diffusion rate of CRFR2 but not of CRFR1. This was uniformly seen regardless of whether FCS or FRAP was used. Different responses have also been noted previously: lateral mobility of A_{2A}-adenosine receptors was not affected upon receptor activation, whereas agonist treatment decreased that of the D_2 receptor

(Charalambous et al., 2008) and increased the mobility of the 5-HT_{1A}-receptor (Pucadyil et al., 2004). It is not clear why receptor mobility changes in an unpredictable way upon agonist occupancy. FCS allowed us to extract information on the mobility of single receptors and showed that the diffusion coefficients varied widely. The basis for this anisotropy is also not clear, but it is indicative of some local confinement of receptors: hypothetical lipid rafts are obvious candidates. Both G protein-coupled receptors (Perez et al., 2006) and G proteins have been found to be enriched in microdomains (Abankwa and Vogel, 2007); most importantly, these microdomains have been found to be substantially more diverse in nature than anticipated from the lipid raft hypothesis (Abankwa and Vogel, 2007). Cortical actin is also required to maintain spatial segregation of membrane domains by organizing fencing (submembranous adapter) and picketing (transmembrane) molecules (Cheng and Miller, 2001; Suzuki et al., 2005). In addition, in some instances, cholesterol is not tolerated in the immediate vicinity of transmembrane proteins. Thus, cholesterol promotes picketing of membrane microdomains by transmembrane proteins, and removal of cholesterol has the reverse effect. Disruption of the actin cytoskeleton abolished the agonist-induced shift to rapidly diffusing species of CRFR2. This observation argues for actin-supported anisotropy of the membrane. It is less clear why depletion or aggregation of cholesterol had a similar effect. The lipid raft hypothesis predicts that cholesterol extraction should accelerate diffusion, an effect that has been observed previously with the A_{2A} adenosine receptor (Charalambous et al., 2008), but it fails to account for the loss of agonist-induced shift to rapid diffusion of CRFR2 and why CRFR1 and CRFR2 should be different. Cholesterol may play a structural role for some GPCRs: in crystals prepared from metarhodopsin-I, cholesterol is trapped within the transmembrane core of the protein (Ruprecht et al., 2004). Likewise, crystal packing of the β_2-adrenergic receptor is apparently facilitated by cholesterol (Cherezov et al., 2007).We therefore propose that the different response to agonist occupancy of CRFR1 and CRFR2 is accounted for by differences in the hydrophobic core of the two receptors, which affects their ability to accommodate cholesterol. Despite their high homology, the TM segments of CRFR1 and CRFR2 show subtle differences: there is, for instance, an excess of bulky side chains in TM1 of CRFR1 (two isoleucines replacing valines) and the corresponding substitutions in TM4 of CRFR2. It is worth noting that the conformational change induced by

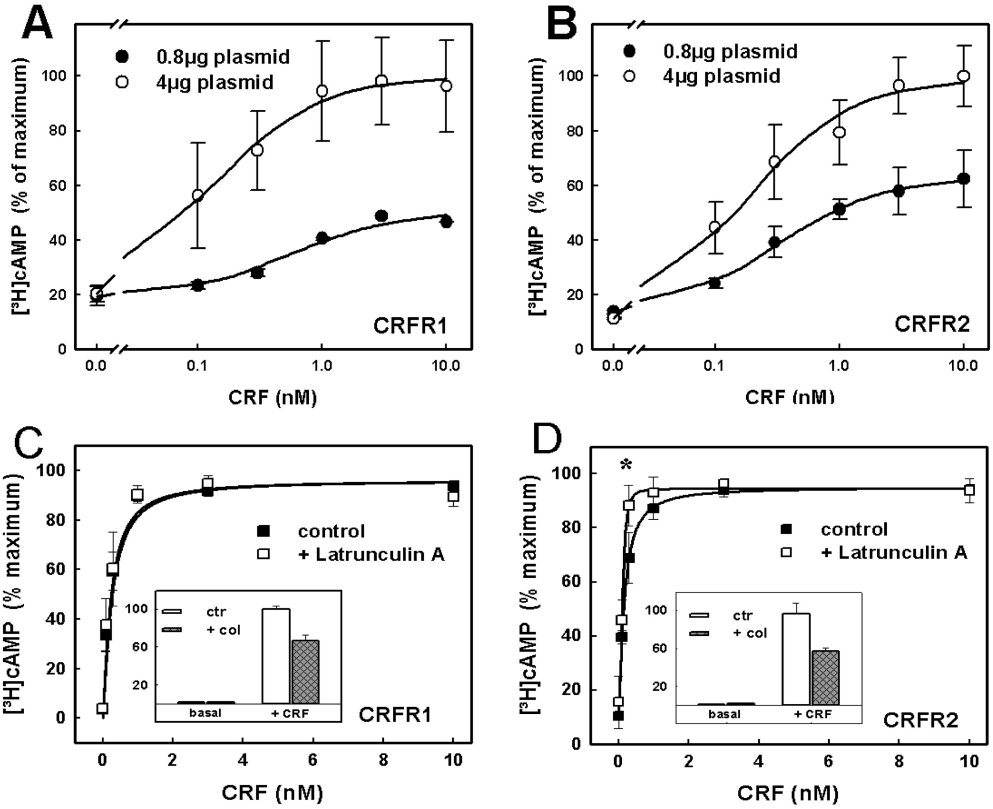

Fig. 11. cAMP accumulation induced by CRFR1 and CRFR2 expressed at different levels (A and B) and after pretreatment of HEK 293 cells with latrunculin (C and D). A and B, HEK 293 cells (6×10^6 cells) were transiently transfected with 0.8 (closed symbol) or 4 μg of plasmid (open symbol) encoding YFP-tagged CRFR1 (A) or CRFR2 (B). Cells (3×10^5 cells/six-well dish) were seeded 24 h after transfection and allowed to adhere for 8 h. Subsequently, the cells were incubated in medium containing pertussis toxin (100 ng/ml) and [^{3}H]adenine (1 μCi/ml) overnight. Cells were subsequently stimulated with CRF for 20 min, and the formation of [^{3}H]cAMP was quantified as outlined in the legend to Fig. 1. EC_{50} values were (means ± S.D.): 0.56 ± 0.11 and 0.12 ± 0.07 nM for low and high CRFR1 expression, respectively ($p = 0.0027$; t test for paired data); 0.29 ± 0.10 and 0.21 ± 0.05 for low and high CRFR2 expression, respectively ($p = 0.10$; t test for paired data). C and D, stably transfected HEK 293 cells expressing CRFR1 (C) or CRFR2 (D) were prelabeled with [^{3}H]adenine overnight and then pretreated with latrunculin A as in Fig. 7 for 1 h before the addition of agonist for 20 min. EC_{50} values for CRF were 0.21 ± 0.05 and 0.22 ± 0.08 (CRFR1; $p = 0.92$) and 0.21 ± 0.04 and 0.14 ± 0.03 nM (CRFR2; $p = 0.04$). Data points represent mean values ± S.D. from 3 (A and B) and 5 (C and D) independent experiments (done in triplicate); maximal [^{3}H]cAMP accumulation in each experiment was set at 100% to account for interassay variation. These 100% values varied from 600 cpm (low receptor expression) to 5000 cpm (stable cell lines expressing CRFR1).

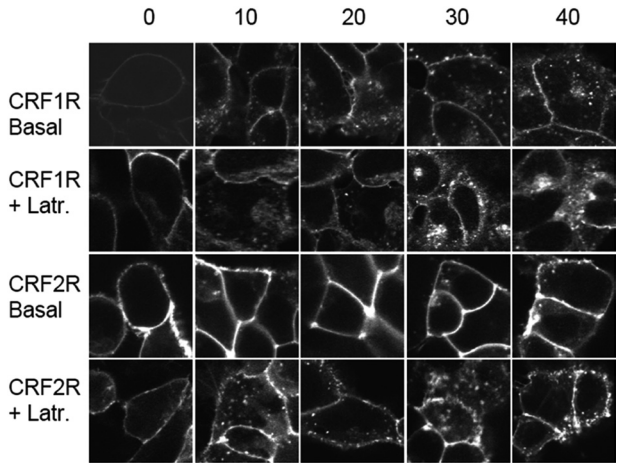

Fig. 12. Agonist-induced internalization of CRFR1 and of CRFR2 in the presence or absence of latrunculin A. HEK 293 cells stably expressing CRFR1 or CRFR2 tagged with YFP were seeded on cover slips and pretreated with vehicle or latrunculin (row labeled + Latr.) as in Fig. 8. Images were captured under basal conditions (time point 0 min) using the 514-nm laser line of a Zeiss 501 confocal laser scanning microscope (see *Materials and Methods*). Subsequently, CRF was added in a concentration of 100 nM, and images were captured in intervals of 10 min in the presence or absence of latrunculin A, laser power was set to 6% with the exception of row "CRF2R Basal": here, laser intensity was set to 11% to visualize all possible intracellular fluorescent particles. Shown are representative images captured in parallel in the same experiment (and replicated with three coverslips each); the experiment was repeated twice.

agonist in CRFR2 caused a structural rearrangement large enough to affect FRET in CRFR2, whereas this was not the case in CRFR1. FIDA unequivocally demonstrated that this enhanced FRET was not due to a change in the oligomeric stoichiometry. Thus, CRFR2 and CRFR1 react to the same agonist and the same cognate G protein(s) with a subtle difference in conformation.

We noted that on average, CRFRs moved faster in hippocampal neurons (Fig. 5) than in HEK 293 cells (e.g., 5.8 ± 3.4 and $9.7 \pm 4.5 \times 10^{-9}$ cm^2/s for CRFR2 expressed in HEK 293 cells and in neurons, respectively). This was surprising, because neurons are believed to contain a large array of adapters linking membrane proteins to the cytoskeleton. Thus, picketing and fencing from the cytoskeleton is expected to be more pronounced in neuronal cells. However, it is worth noting that we examined the mobility of the receptors over the somatic region and that these neurons did not form extensive synapses. It is likely that picketing and fencing of some areas of the membrane requires synaptic input to organize the actin cytoskeleton. Large variations were also noted for the β_2-adrenergic receptor when expressed in A549 cells, allowing for the resolution of two components (28.8 ± 17.2 and $1.1 \pm 0.46 \times 10^{-9}$ cm^2/s); it is important to note that the mobility of the β_2-adrenergic receptors was higher when expressed in hippocampal neurons than in A549 cells (Hegener et al., 2004). Most importantly, in hippocampal neurons, CRF again promoted a shift in the distribution of CRFR2—but not of CRFR1—in favor of the rapidly migrating species. Thus, the variation in diffusion coefficients that we observed is probably representative of the possible range of mobility, which occurs in the intact organism. We are also confident that the observations faithfully reproduce intrinsic differences in the response of the two receptor subtypes, which are important in vivo.

Acknowledgments

We thank Helmut Kubista for help with the preparation of hippocampal neurons, Marion Holy for excellent technical assistance, and Johannes A. Schmid for help with FRAP analysis and insightful comments.

References

Abankwa D and Vogel H (2007) A FRET map of membrane anchors suggests distinct microdomains of heterotrimeric G proteins. *J Cell Sci* **120:**2953–2962.

Adkins EM, Samuvel DJ, Fog JU, Eriksen J, Jayanthi LD, Vaegter CB, Ramamoorthy S, and Gether U (2007) Membrane mobility and microdomain association of the dopamine transporter studied with fluorescence correlation spectroscopy and fluorescence recovery after photobleaching. *Biochemistry* **46:**10484–10497.

Allen JA, Halverson-Tamboli RA, and Rasenick MM (2007) Lipid raft microdomains and neurotransmitter signaling. *Nat Rev Neurosci* **8:**128–140.

Bacia K and Schwille P (2003) A dynamic view of cellular processes by in vivo fluorescence auto- and cross-correlation spectroscopy. *Methods* **29:**74–85.

Barak LS, Ferguson SS, Zhang J, and Caron MG (1997) A β-arrestin green fluorescent protein biosensor for detecting G protein-coupled receptor activation. *J Biol Chem* **272:**27497–27500.

Bartholomäus I, Milan-Lobo L, Nicke A, Dutertre S, Hastrup H, Jha A, Gether U, Sitte HH, Betz H, and Eulenburg V (2008) Glycine transporter dimers: evidence for occurrence in the plasma membrane. *J Biol Chem* **283:**10978–10991.

Briddon SJ, Middleton RJ, Cordeaux Y, Flavin FM, Weinstein JA, George MW, Kellam B, and Hill SJ (2004) Quantitative analysis of the formation and diffusion of A_1-adenosine receptor-antagonist complexes in single living cells. *Proc Natl Acad Sci U S A* **101:**4673–4678.

Brock C, Oueslati N, Soler S, Boudier L, Rondard P, and Pin JP (2007) Activation of a dimeric metabotropic glutamate receptor by intersubunit rearrangement. *J Biol Chem* **282:**33000–33008.

Charalambous C, Gsandtner I, Keuerleber S, Milan-Lobo L, Kudlacek O, Freissmuth M, and Zezula J (2008) Restricted collision coupling of the A_{2A}-receptor revisited: evidence for physical separation of two signaling cascades. *J Biol Chem* **283:**9276–9288.

Chen Y, Lagerholm BC, Yang B, and Jacobson K (2006) Methods to measure the lateral diffusion of membrane lipids and proteins. *Methods* **39:**147–153.

Cheng ZJ and Miller LJ (2001) Agonist-dependent dissociation of oligomeric complexes of G protein-coupled cholecystokinin receptors demonstrated in living cells using bioluminescence resonance energy transfer. *J Biol Chem* **276:**48040–48047.

Cherezov V, Rosenbaum DM, Hanson MA, Rasmussen SG, Thian FS, Kobilka TS, Choi HJ, Kuhn P, Weis WI, Kobilka BK, et al. (2007) High-resolution crystal structure of an engineered human β_2-adrenergic G protein coupled receptor. *Science* **318:**1258–1265.

Chini B and Parenti M (2004) G protein coupled receptors in lipid rafts and caveolae: how, when and why do they go there? *J Mol Endocrinol* **32:**325–338.

Cvejic S and Devi LA (1997) Dimerization of the δ-opioid receptor: implication for a role in receptor internalization. *J Biol Chem* **272:**26959–26964.

Edetsberger M, Gaubitzer E, Valic E, Waigmann E, and Köhler G (2005) Detection of nanometer-sized particles in living cells using modern fluorescence fluctuation methods. *Biochem Biophys Res Commun* **332:**109–116.

Ernst OP, Gramse V, Kolbe M, Hofmann KP, and Heck M (2007) Monomeric G protein-coupled receptor rhodopsin in solution activates its G protein transducin at the diffusion limit. *Proc Natl Acad Sci U S A* **104:**10859–10864.

Fredriksson R, Lagerström MC, Lundin LG, and Schiöth HB (2003) The G protein-coupled receptors in the human genome form five main families. Phylogenetic analysis, paralogon groups, and fingerprints. *Mol Pharmacol* **63:**1256–1272.

Freissmuth M, Casey PJ, and Gilman AG (1989) G-Proteins control diverse pathways of transmembrane signaling. *FASEB J* **3:**2125–2131.

Haupts U, Maiti S, Schwille P, and Webb WW (1998) Dynamics of fluorescence fluctuations in green fluorescent protein observed by fluorescence correlation spectroscopy. *Proc Natl Acad Sci U S A* **95:**13573–13578.

Head BP, Patel HH, Roth DM, Murray F, Swaney JS, Niesman IR, Farquhar MG, and Insel PA (2006) Microtubules and actin microfilaments regulate lipid raft/caveolae localization of adenylyl cyclase signaling components. *J Biol Chem* **281:**26391–26399.

Hegener O, Prenner L, Runkel F, Baader SL, Kappler J, and Häberlein H (2004) Dynamics of β_2-adrenergic receptor—ligand complexes on living cells. *Biochemistry* **43:**6190–6199.

Hein P, Frank M, Hoffmann C, Lohse MJ, and Bünemann M (2005) Dynamics of receptor/G protein coupling in living cells. *EMBO J* **24:**4106–4114.

Hlavackova V, Goudet C, Kniazeff J, Zikova A, Maurel D, Vol C, Trojanova J, Prézeau L, Pin JP, and Blahos J (2005) Evidence for a single heptahelical domain being turned on upon activation of a dimeric GPCR. *EMBO J* **24:**499–509.

Just H, Sitte HH, Schmid JA, Freissmuth M, and Kudlacek O (2004) Identification of an additional interaction domain in transmembrane domains 11 and 12 that supports oligomer formation in the human serotonin transporter. *J Biol Chem* **279:**6650–6657.

Kask P, Palo K, Ullmann D, and Gall K (1999) Fluorescence-intensity distribution analysis and its application in biomolecular detection technology. *Proc Natl Acad Sci U S A* **96:**13756–13761.

Kudlacek O, Mitterauer T, Nanoff C, Hohenegger M, Tang WJ, Freissmuth M, and Kleuss C (2001) Inhibition of adenylyl and guanylyl cyclase isoforms by the antiviral drug foscarnet. *J Biol Chem* **276:**3010–3016.

Maier C, Rünzler D, Schindelar J, Grabner G, Waldhäusl W, Köhler G, and Luger A (2005) G-Protein-coupled glucocorticoid receptors on the pituitary cell membrane. *J Cell Sci* **118:**3353–3361.

Perez JB, Segura JM, Abankwa D, Piguet J, Martinez KL, and Vogel H (2006) Monitoring the diffusion of single heterotrimeric G proteins in supported cell-

membrane sheets reveals their partitioning into microdomains. *J Mol Biol* **363:** 918–930.
Pfleger KD and Eidne KA (2005) Monitoring the formation of dynamic G-protein-coupled receptor-protein complexes in living cells. *Biochem J* **385:**625–637.
Philip F, Sengupta P, and Scarlata S (2007) Signaling through a G protein-coupled receptor and its corresponding G protein follows a stoichiometrically limited model. *J Biol Chem* **282:**19203–19216.
Pin JP, Neubig R, Bouvier M, Devi L, Filizola M, Javitch JA, Lohse MJ, Milligan G, Palczewski K, Parmentier M, et al. (2007) International Union of Basic and Clinical Pharmacology. LXVII. Recommendations for the recognition and nomenclature of G protein-coupled receptor heteromultimers. *Pharmacol Rev* **59:**5–13.
Pucadyil TJ, Kalipatnapu S, Harikumar KG, Rangaraj N, Karnik SS, and Chattopadhyay A (2004) G-protein-dependent cell surface dynamics of the human serotonin1A receptor tagged to yellow fluorescent protein. *Biochemistry* **43:**15852–15862.
Puthenveedu MA and von Zastrow M (2006) Cargo regulates clathrin-coated pit dynamics. *Cell* **127:**113–124.
Ruprecht JJ, Mielke T, Vogel R, Villa C, and Schertler GFX (2004) Electron crystallography reveals the structure of metarhodopsin I. *EMBO J* **23:**3609–3620.
Suzuki K, Ritchie K, Kajikawa E, Fujiwara T, and Kusumi A (2005) Rapid hop diffusion of a G-protein-coupled receptor in the plasma membrane as revealed by single-molecule techniques. *Biophys J* **88:**3659–3680.
Waldhoer M, Wise A, Milligan G, Freissmuth M, and Nanoff C (1999) Kinetics of ternary complex formation with fusion proteins composed of the A_1-adenosine receptor and G protein α-subunits. *J Biol Chem* **274:**30571–30579.
Whetton AD, Gordon LM, and Houslay MD (1983) Elevated membrane cholesterol concentrations inhibit glucagon-stimulated adenylate cyclase. *Biochem J* **210:**437–449.
Whorton MR, Bokoch MP, Rasmussen SG, Huang B, Zare RN, Kobilka B, and Sunahara RK (2007) A monomeric G protein-coupled receptor isolated in a high-density lipoprotein particle efficiently activates its G protein. *Proc Natl Acad Sci U S A* **104:**7682–7687.
Wietfeld D, Heinrich N, Furkert J, Fechner K, Beyermann M, Bienert M, and Berger H (2004) Regulation of the coupling to different G proteins of rat corticotropin-releasing factor receptor type 1 in human embryonic kidney 293 Cells. *J Biol Chem* **279:**38386–38394.
Yguerabide J, Schmidt JA, and Yguerabide EE (1982) Lateral mobility in membranes as detected by fluorescence recovery after photobleaching. *Biophys J* **40:** 69–75.

Address correspondence to: Dr. Michael Freissmuth, Medical University of Vienna, Center for Biomolecular Medicine and Pharmacology, Institute of Pharmacology, Waehringerstrasse 13a, A-1090 Vienna, Austria. E-mail: michael.freissmuth@meduniwien.ac.at